Original Article

A novel necroptosis-related miRNA signature for predicting the prognosis of esophageal cancer and immune infiltration analysis

Miao Zhang[1,2#], Shaoran Song[3#], Bo Wang[1,2], Yangyang Shang[1,2], Peijun Liu[1,2], Juan Li[1,2]

[1]Center for Translational Medicine, the First Affiliated Hospital of Xi'an Jiaotong University, Xi'an, China; [2]Key Laboratory for Tumor Precision Medicine of Shaanxi Province, the First Affiliated Hospital of Xi'an Jiaotong University, Xi'an, China; [3]Department of Radiotherapy, Shaanxi Provincial People's Hospital, Xi'an, China

Contributions: (I) Conception and design: J Li, P Liu; (II) Administrative support: None; (III) Provision of study materials or patients: J Li; (IV) Collection and assembly of data: M Zhang, B Wang, Y Shang; (V) Data analysis and interpretation: M Zhang, S Song; (VI) Manuscript writing: All authors; (VII) Final approval of manuscript: All authors.

[#]These authors contributed equally to this work.

Correspondence to: Juan Li, PhD; Peijun Liu, PhD. Center for Translational Medicine, the First Affiliated Hospital of Xi'an Jiaotong University, 277 Yanta Western Road, Xi'an 710061, China; Key Laboratory for Tumor Precision Medicine of Shaanxi Province, the First Affiliated Hospital of Xi'an Jiaotong University, Xi'an 710061, China. Email: lijuanxjtu@xjtu.edu.cn; liupeijun@xjtu.edu.cn.

Background: The prognostic value of necroptosis-related microRNAs (miRNAs), which are important in tumorigenesis and development, remains unclear. Therefore, we aimed to screen prognostic necroptosis-related miRNAs in esophageal cancer (EC).

Methods: Nine necroptosis-related miRNA expression profiles and associated clinical data of EC patients were obtained from The Cancer Genome Atlas (TCGA) database. The relationships between necroptosis-related miRNAs and overall survival (OS) were determined via Cox regression model analysis. Target genes of the miRNAs were investigated in TargetScan, miRDB, and miRTarBase. The biological functions of these genes were evaluated by Gene Ontology (GO) and Kyoto Encyclopedia of Genes and Genomes (KEGG) analyses. For the most significant correlation between miR-425-5p expression and the survival of EC patients, the effect of miR-425-5p on necroptosis was explored in EC cells. The relationship between targeted gene expression and immune infiltration was also analyzed and validated.

Results: Hsa-miR-425-5p, hsa-miR-500a-3p, hsa-miR-7-5p and hsa-miR-200a-5p were selected for the construction of a prognostic signature based on their correlation with the survival of EC patients. EC patients were divided into high- and low-risk groups according to the median value of the risk score. Patients in the high-risk group tended to have higher death rates than those in the low-risk group ($P<0.05$). The risk score was an independent prognostic indicator for the OS of EC patients [hazard ratio (HR) >1, $P<0.05$]. The prognostic model had good predictive efficiency. The genes targeted by necroptosis-related miRNAs were significantly enriched in apoptosis etc. The inhibition of miR-425-5p promoted necroptosis in EC cells by targeting branched chain amino acid transaminase 1 (*BCAT1*). The expression level of *BCAT1* was significantly correlated with immune infiltration.

Conclusions: A necroptosis-related four-miRNA model was constructed successfully to predict the potential value of the four miRNAs in the prognosis of EC, which can be conducive to promoting the therapeutic effect on EC.

Keywords: Esophageal cancer (EC); necroptosis; miRNA signature; prognosis

Submitted Aug 27, 2024. Accepted for publication Dec 26, 2024. Published online Feb 26, 2025.
doi: 10.21037/tcr-24-1532
View this article at: https://dx.doi.org/10.21037/tcr-24-1532

Introduction

Esophageal cancer (EC) is a significant contributor to cancer-related mortality on a global scale. According to global cancer statistics released in 2022, EC ranks as the seventh leading cause of cancer mortality and the eleventh most prevalent cancer, with 445,129 deaths and 510,716 new cases reported (1). The prognosis for advanced EC remains poor, with a 5-year relative survival rate of only 5.2% (2). Several risk factors have been identified for EC, including gastroesophageal reflux disease, alcohol consumption, smoking, obesity and body composition (3). Most patients have advanced or metastasized disease at diagnosis (4). Thus, it is crucial to develop innovative prognostic prediction methods for EC patients to identify those at high risk effectively.

Necroptosis, originally proposed in 2005, is a form of programmed cell death with the characteristics of activation of autophagy and necrotic cell death morphology (5). Previous studies have shown that necroptosis has dual roles in cancer development (6,7). A study has suggested the suppressive role of necroptosis (8), whereas other studies have reported that necroptosis may be a tumor promoter in tumor development (9,10). The influence of the expression of necroptotic factors on cancer prognosis also varies across different cancers. Low receptor interacting serine/threonine-protein kinase (*RIPK*)-3 expression is correlated with a poor prognosis in breast cancer patients (8) and reduced overall survival (OS) and disease-free survival (DFS) in colorectal cancer patients (11). However, in low-grade gliomas, higher expression of *RIPK1*, *RIPK3* and mixed lineage kinase domain-like protein (*MLKL*) indicates a poorer prognosis (12). A high level of pMLKL is markedly correlated with poor prognosis in patients with esophageal squamous cell carcinoma (ESCC) (13). Even so, the understanding of the role of necroptosis in the prognosis of EC is still limited and needs to be further clarified.

MicroRNAs (miRNAs), small endogenous noncoding RNAs, play a key role in tumor progression. MiRNAs can bind directly to target mRNAs and then regulate gene expression at the post-translational level (14). Overexpression of miRNA-96-5p reduces the expression of the tumor suppressor gene forkhead box protein O3 (*FOXO3*) (15), which may play a tumor promoting role in breast cancer. MiRNA-29b significantly inhibits tumor growth and induces apoptotic cell death by inducing the expression of the proapoptotic molecule bcl2-interacting mediator of cell death (*Bim*), cytochrome C release and poly [ADP-ribose] polymerase (*PARP*) cleavage in prostate cancer (16), which acts as a tumor suppressor. In EC, miRNA-485-5p suppresses tumorigenesis by suppressing the proliferation, migration, and invasion of EC cells (17), whereas the overexpression of novel-miR-4885 (18) and miR-3682-3p (19) can attenuate EC cell proliferation, migration, and invasion. There are also several miRNAs that can be used to predict the prognosis of EC patients, such as miR-1972, miR-4274, miR-4701-3p, miR-6126 and miR-1268a (20). However, little is known regarding the relationship between necroptosis-related miRNAs and the prognosis of EC patients.

In our study, we established and validated a prognostic necroptosis-related miRNA signature of EC, in which the miRNA expression profiles and corresponding clinical data of EC patients were obtained from The Cancer Genome Atlas (TCGA) database. Furthermore, we further explored the target genes of the prognostic miRNAs and performed functional enrichment analysis. Flow cytometry and real-time polymerase chain reaction (PCR) were used to detect the effects of miR-425-5p, the most significantly correlated miRNA with the survival of EC patients, on necroptosis in EC cells. We also explored the relationship

Highlight box

Key findings

- We successfully constructed a necroptosis-related microRNA (miRNA) signature to effectively predict the prognosis of esophageal cancer (EC) patients, which consists of hsa-miR-425-5p, hsa-miR-500a-3p, hsa-miR-7-5p and hsa-miR-200a-5p.
- The risk score was proved to be an independent prognostic indicator for the overall survival of EC patients.
- The inhibition of miR-425-5p promoted necroptosis in EC cells by targeting branched chain amino acid transaminase 1 (*BCAT1*). The inhibition of *BCAT1* significantly reduced *CD274* expression.

What is known and what is new?

- According to the reports, necroptosis plays an important role in cancer development. The understanding of the role of necroptosis in prognosis of EC is still limited and needs to be further clarified.
- We developed a prognosis prediction model based on necroptosis-related miRNAs in EC. MiR-425-5p decreased necroptosis of EC cells by increasing *BCAT1* expression. *BCAT1* was significantly correlated with immune infiltration.

What is the implication, and what should change now?

- This model can predict the prognosis of EC patients more accurately and provide new theoretical basis for finding the potential therapy target of EC. MiR-425-5p and its target gene *BCAT1* may be up-and-coming therapy targets.

between targeted gene expression and immune infiltration. We present this article in accordance with the TRIPOD reporting checklist (available at https://tcr.amegroups.com/article/view/10.21037/tcr-24-1532/rc).

Methods

Data collection

We collected miRNA sequencing data from the TCGA database, which included 196 samples (183 EC samples and 13 non-cancer samples). The corresponding clinical information was also downloaded. All the data from TCGA are publicly available. By performing R language (version 4.1.1), the miR-seq transcriptomic data were normalized to transcripts per kilobase million (TPM) values for further analysis by using the Edge R package. The study was conducted in accordance with the Declaration of Helsinki (as revised in 2013).

Necroptosis-related miRNA definition

A total of thirteen necroptosis-related miRNAs were obtained from a prior study (21), only nine of which exist in the miRNA expression profile of the TCGA-EC database. The expression matrix and correlation of differentially expressed miRNAs in EC and normal tissues were analysed by the "limma" package. The adj.P.vals (adjusted P values) were obtained by using Benjamini Hochberg method for multiple comparison correction to control the false discovery rate (FDR).

Construction and verification of the prognostic necroptosis-related miRNA signature

The "caret" package was utilized to separate the 183 EC patients randomly into training and testing groups at a ratio of 2 to 1. The prognostic value of necroptosis-related miRNAs was estimated by univariate Cox analysis in the training cohort using the R "survival" package. Least absolute shrinkage and selection operator (LASSO) regression via the "glmnet" R package was used to establish the prognostic model. Four survival-related miRNAs and their coefficients (β) were subsequently acquired for further study. The minimum criteria were used to determine the penalty parameter λ values. The EC patients were separated into either a low- or high-risk subgroup based on the median risk score. The formula for deriving the risk score was as follows: miRNA signature risk score = expression of miRNA1 × β1 + expression of miRNA2 × β2 +... expression of miRNAn × βn. The "survminer" R package and the "survivalROC" R package were used to analyse the survival rate and the predictive efficacy between the two risk groups. Moreover, univariate and multivariate Cox regression analyses were utilized to explore whether the risk score of our model has independent prognostic value.

Functional enrichment analysis

The target genes of the four miRNAs (hsa-miR-425-5p, hsa-miR-500a-3p, hsa-miR-7-5p and hsa-miR-200a-5p) were acquired from three databases (miRDB: http://www.mirdb.org/, miRTarBase: http://mirtarbase.mbc.nctu.edu.tw//, TargetScan: http://www.targetscan.org//). The network interrelation of the common genes was charted by Cytoscape_v3.9.1. The "clusterProfiler" package was applied to perform Gene Ontology (GO) and Kyoto Encyclopedia of Genes and Genomes (KEGG) analyses. The adj.P.vals were obtained by using Benjamini Hochberg method for multiple comparison correction to control the FDR.

Cell culture

Human EC cells EC109 and EC9706 were purchased from the Hunan Fenghui Biotechnology Co., Ltd. (Changsha, China). RPMI 1640 medium was used to culture EC109 and EC9706, in which 10% fetal bovine serum (FBS) and 1% penicillin-streptomycin supplied. The cells were placed in a humidified incubator at 37 ℃ containing 5% CO_2. The medium was renewed every other day.

Flow cytometry

The cells were digested with trypsin and collected. The cells were resuspended in binding buffer after being washed with phosphate buffered solution (PBS). FITC-conjugated anti-annexin V antibodies and 7-AAD (R&D Systems) were used for cell staining. Flow cytometry analysis was performed by using a FACSCalibur flow cytometer (Becton, Dickinson and Company, New Jersey, USA).

RNA isolation and real-time PCR

A miRcute miRNA Isolation Kit (DP501, TIANGEN) was used for the isolation of miRNAs. Following the

instructions of the miDETECT A Track miRNA qRT-PCR Starker Kit (C10712, RIB-BIO), all the miRNAs were polyadenylated by poly(A) polymerase and converted into cDNA. An RNA Fast 200 isolation kit (220010, Feijie) was used for the extraction of total RNA, which was converted to cDNA using cDNA Reverse Transcription Premix (11123, Yeasen). Real-time PCR was conducted with qPCR SYBR Green Master Mix (11201, Yeasen). MiRNA expression was normalized to U6, mRNA expression was determined by normalization to glyceraldehyde-3-phosphate dehydrogenase (GAPDH). All primers used were obtained from Sangon Biotech (Shanghai, China).

Immune infiltration analysis

The gene set variation analysis (GSVA) enrichment analysis was performed to estimate the differences in biological pathways by using the "GSVA" R package. The single-sample gene set enrichment analysis (ssGSEA) algorithm was used to evaluate the fractions of 23 human immune cell subsets in different branched chain amino acid transaminase 1 (*BCAT1*) expression groups of EC, which conducted by Spearman test. The expression of 33 critical immune checkpoints retrieved from previous research was compared in *BCAT1* low- and high-expression group, which conducted by Wilcoxon rank-sum test.

Immunohistochemistry (IHC)

IHC staining was performed with EC tissue microarray (Outdo Biotechnology, Shanghai, China). We used a Biotin-Streptavidin Horseradish Peroxidase (HRP) Detection System (ZSGB-BIO, Beijing, China) to perform IHC staining. Images were taken by a Leica SCN400 slide scanner (Germany). The primary antibodies used for IHC included BCAT1 (Proteintech) and lymphocyte antigen 6G (Ly6G) (Invitrogen). The scoring method for BCAT1 expression was as follows: ten random visual fields were selected for each tissue slice, and semiquantitative scoring was used for the estimation of tissue staining in each visual field. Positive cell rate integration method: if there were no positive cells or the proportion of positive cells was less than 10%, 0 points were counted; positive cells accounted for 10% to 25%, 1 point was counted; positive cells accounted for 26–50%, 2 points; positive cells accounted for 51–75%, 3 points; positive cell ratio >75%, 4 points. The dyeing intensity integration method was as follows: no staining of cells, 0 points; light yellow color, 1 point; brown yellow color, 2 points; brown color, 3 points. The result was determined by the product of the positive cell rate and staining intensity: a product of 0 indicated negative (–), and a product of 1–4 indicated weak positive (+); a product of 5–8 was recorded as positive (++); a product of 9–12 was recorded as strongly positive (++). The number of Ly6G-positive cells was analyzed by Image J.

Western blotting

Protein extraction was performed with radio immunoprecipitation assay (RIPA) lysis buffer containing protease and phosphatase inhibitors, and Bio-Rad protein assay reagent (Bio-Rad) was used to estimate the protein concentration. Cell extracts were separated by sodium dodecyl sulfate-polyacrylamide gel electrophoresis (SDS-PAGE) and transferred to polyvinylidene difluoride membranes (PVDF, Millipore). Subsequently, the membranes were blocked with 5% fat-free milk in TBST for an hour to prevent non-specific binding and then incubated with primary antibody overnight at 4 ℃. Primary antibodies used in Western blotting included BCAT1 (Proteintech), programmed cell death 1 ligand 1 (PD-L1) (Cell Signaling Technology) and GAPDH (Proteintech). The next day, the membranes were cleaned and incubated with horseradish peroxidase-conjugated secondary antibody for an hour at room temperature (Proteintech). Chemiluminescent signals were detected using electrochemiluminescence (Bio-Rad).

Statistical analysis

Data analysis was performed with R language version 4.1.1 or GraphPad Prism 9, and all experiments were repeated at least 3 times. These results were presented as the mean ± standard deviation (SD). Student's two-sided *t*-test was used to evaluate the differences between the two groups. Survival analysis between different risk groups was performed by Kaplan-Meier curves with the log-rank test. Univariate and multivariate Cox regression analyses were utilized to explore the independent predictors of OS. Statistical significance was considered as $P<0.05$.

Results

The flow chart of the construction and validation of data collection and analysis in this study is shown in *Figure 1*. A total of 183 EC patients in the TCGA database were included in this work.

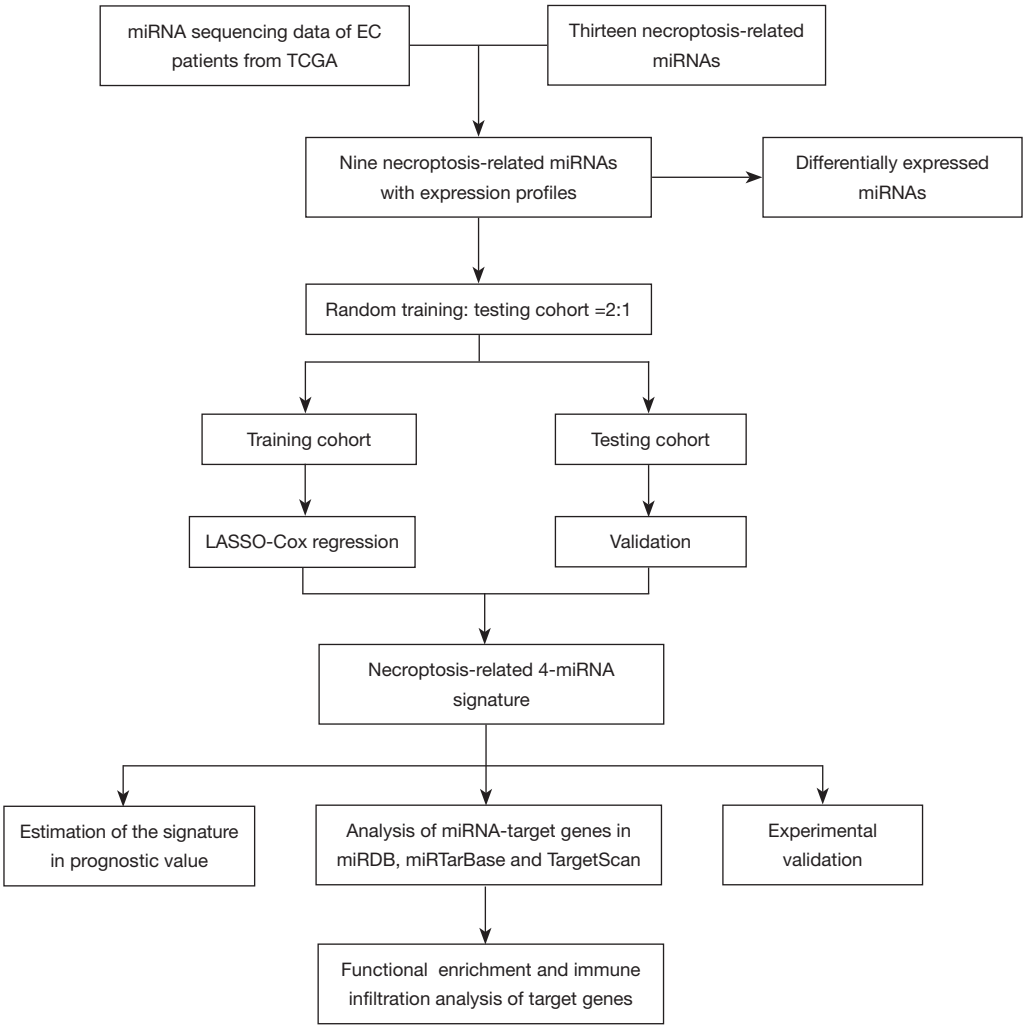

Figure 1 Flow chart of the study. miRNA, microRNA; EC, esophageal cancer; TCGA, The Cancer Genome Atlas; LASSO, least absolute shrinkage and selection operator.

Overview of nine necroptosis-related miRNAs

Thirteen necroptosis-related miRNAs were obtained from a previous study, while only 9 of them owned miRNA expression profiles in the TCGA-EC database. The expression levels and distributions of these nine miRNAs (hsa-miR-331-3p, hsa-miR-7-5p, hsa-miR-148a-3p, hsa-miR-141-3p, hsa-miR-200a-5p, hsa-miR-425-5p, hsa-miR-500a-3p, hsa-miR-16-5p, hsa-miR-223-3p) were depicted in the heatmap (*Figure 2A*). Among them, six necroptosis-related miRNAs (hsa-miR-331-3p, P=0.002; hsa-miR-7-5p, P=0.03; hsa-miR-148a-3p, P=0.002; hsa-miR-425-5p, P=0.002; hsa-miR-16-5p, P<0.001; hsa-miR-223-3p, P=0.01) were screened through differential expression analysis between normal and EC samples ($|\log_2 FC| \geq 0$ and FDR <0.05). We also constructed the correlation network for the nine necroptosis-related miRNAs as shown in *Figure 2B* (red lines represent positive correlation; blue lines represent negative correlation. The deeper the color was, the stronger the relevance).

Establishment of a prognostic necroptosis-related miRNA signature in the TCGA training cohort

The samples were split into two cohorts at a ratio of 2 (training cohort) to 1 (testing cohort) at random. The results of univariate Cox regression analysis of these 9 necroptosis-related miRNAs in training cohort were shown

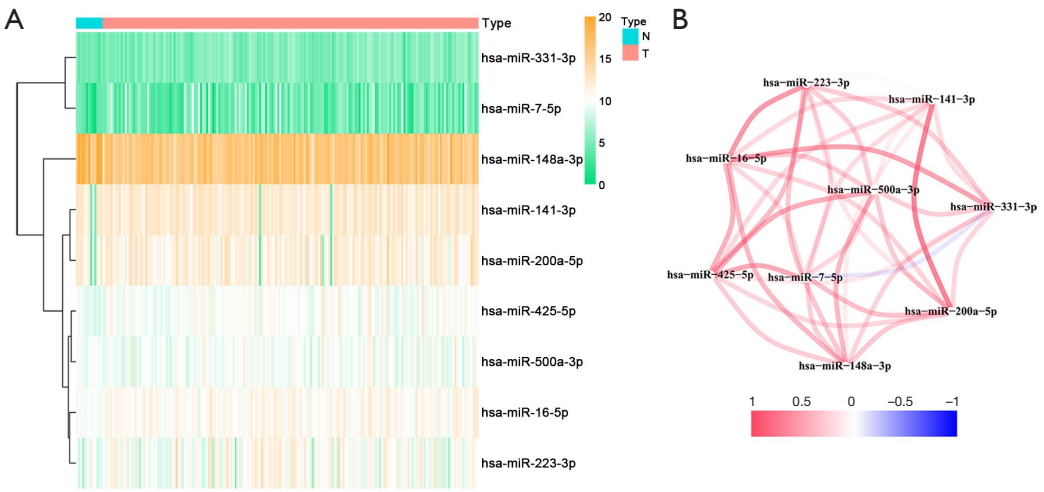

Figure 2 Screening of the nine necroptosis-related miRNAs in the TCGA database. (A) Heatmap of the expression levels and distributions of the nine necroptosis-related miRNAs in normal and esophageal cancer tissues (green: low expression; orange: high expression; N: normal; T: tumor). (B) The correlation network of the nine miRNAs (red line: positive correlation; blue line: negative correlation. The depth of the colour indicates the intensity of the correlation). TCGA, The Cancer Genome Atlas; miRNA, microRNA.

in *Figure 3A*, from which we found that 6 of these miRNAs were risk factors with hazard ratios (HRs) greater than 1 (hsa-miR-148a-3p, hsa-miR-16-5p, hsa-miR-223-3p, hsa-miR-425-5p, hsa-miR-500a-3p, and hsa-miR-7-5p), while the other 3 miRNAs (hsa-miR-141-3p, hsa-miR-200a-5p, and hsa-miR-331-3p) correlated with the favorable survival of EC patients, as indicated by HRs less than 1. LASSO regression analysis was used to build the prognostic model consisting of hsa-miR-425-5p, hsa-miR-500a-3p, hsa-miR-7-5p and hsa-miR-200a-5p according to the minimum criterion optimal λ value (*Figure 3B*,*3C*). The following formula was used to calculate the risk score: risk score = expression of hsa-miR-425-5p × 0.672 + expression of hsa-miR-500a-3p × 0.184 + expression of hsa-miR-7-5p × 0.130 – expression of hsa-miR-200a-5p × 0.432. The patients in the training cohort were stratified into either high- or low-risk subgroups according to the median risk score (*Figure 3D*). Patients with high-risk scores had more deaths, and the survival time was shorter than that of patients in the low-risk group (*Figure 3E*). The Kaplan-Meier survival curve indicated that patients in the high-risk group had a lower OS than those in the low-risk group (P=0.02) (*Figure 3F*). The subsequent time-dependent receiver operating characteristic (ROC) analysis helped us to evaluate the predictive efficacy of the prognostic model. The area under the curve (AUC) reached 0.682 at 1 year, 0.670 at 2 years and 0.733 at 3 years (*Figure 3G*), which demonstrated that the necroptosis-related 4-miRNA risk model could be used to robustly evaluate and predict the survival of EC patients.

Validation of the prognostic risk model

To investigate the efficiency of the risk model constructed above, we performed validation in the testing cohort. According to the median value of risk scores calculated by the same formula in the training cohort, the patients were assigned into the high- and low-risk groups (*Figure 4A*). In the validation cohort, patients with high risk tended to have higher death rates than the low-risk group (*Figure 4B*), which was similar to the results in the training cohort. A significant difference was observed in OS of the low- and high-risk groups by Kaplan-Meier survival curve analysis (P=0.04) (*Figure 4C*). ROC analysis displayed that the AUCs of the 1-, 2-, and 3-year OS were 0.635, 0.701, and 0.622, respectively, indicating that the risk model was reliable (*Figure 4D*). Given that EC is a diverse entity, we evaluated the performance of the model in stratified groups. The 183 EC patients were divided into two groups by histological classification: adenocarcinoma (87 adenocarcinomas, 1 tubular adenocarcinoma, 1 mucinous adenocarcinoma) and squamous cell carcinoma (88 squamous cell carcinoma, 1 basaloid squamous cell carcinoma, 5 squamous cell carcinomas, keratinizing). The adenocarcinoma patients

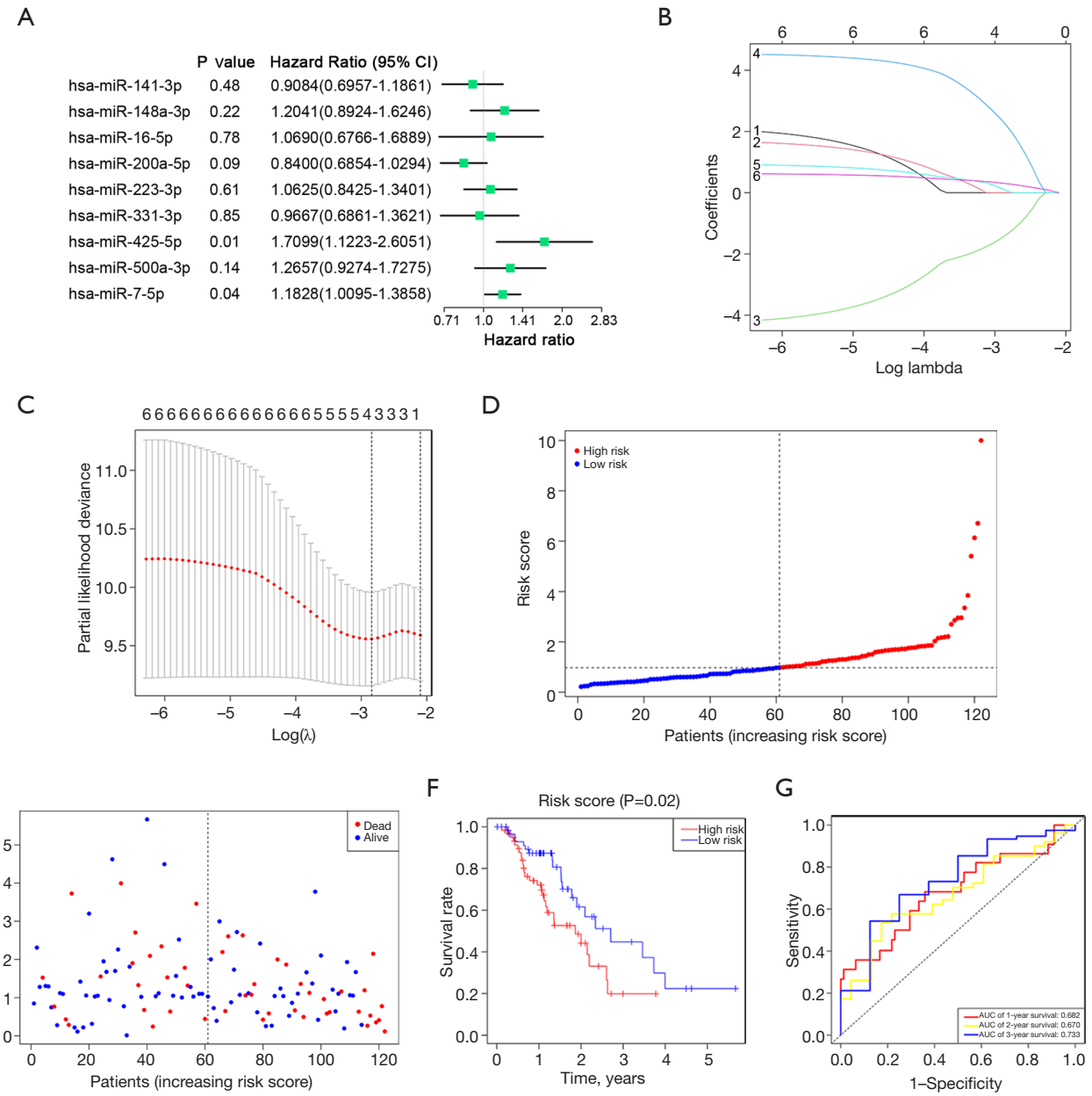

Figure 3 Construction of the necroptosis-related miRNA model in the TCGA training cohort. (A) Forest plots of the univariate Cox regression analysis between the miRNAs and overall survival. (B,C) LASSO regression model of the miRNAs. (D) Distribution of the risk scores in the training cohort. (E) Analysis of the survival status in the training cohort. (F) Kaplan-Meier analysis of the overall survival of esophageal cancer patients in the high- and low-risk groups. (G) AUC of time-dependent ROC curves to evaluate the predictive efficiency. CI, confidence interval; TCGA, The Cancer Genome Atlas; miRNA, microRNA; LASSO, least absolute shrinkage and selection operator; AUC, area under the curve; ROC, receiver operating characteristic.

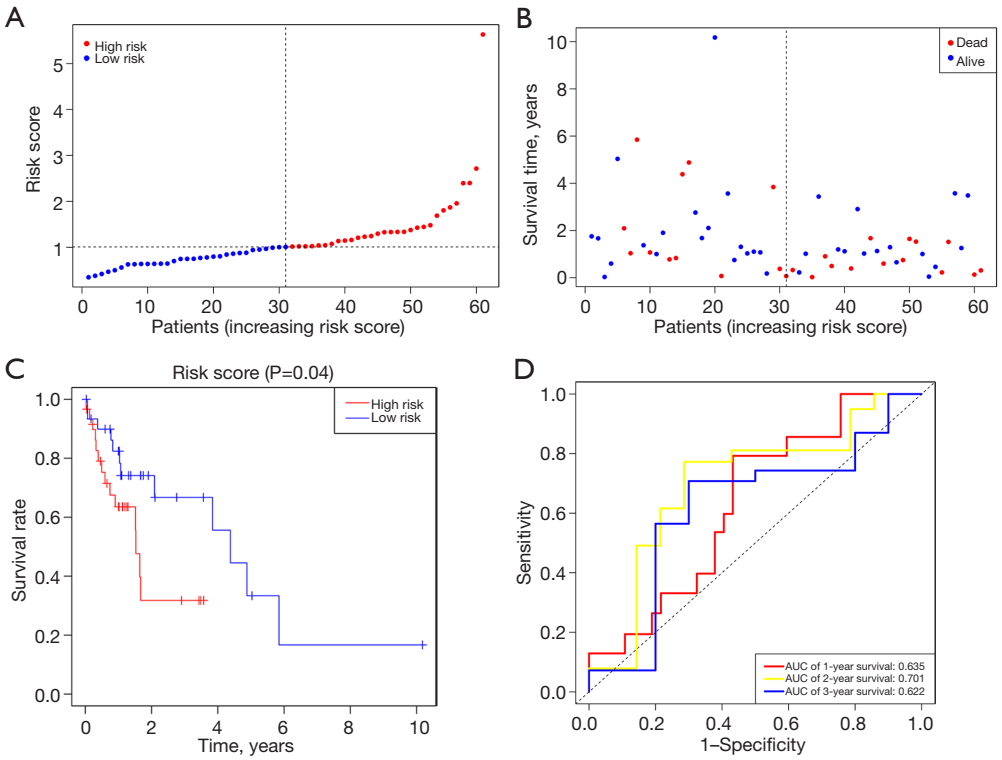

Figure 4 Validation of the risk model in the TCGA testing cohort. (A) Analysis of risk scores in the validation cohort. (B) Distribution of survival status in the validation cohort. (C) Kaplan-Meier survival curves in the high- and low-risk groups. (D) AUCs of time-dependent ROC curves for the 1-, 2-, and 3-year OS in the validation cohort. AUC, area under the curve; TCGA, The Cancer Genome Atlas; ROC, receiver operating characteristic; OS, overall survival.

were assigned into low- and high-risk groups respectively according to the median risk score calculated by the same formula (Figure S1A). The survival status, Kaplan-Meier survival curve and ROC analysis were performed similarly. The adenocarcinoma patients with high risk had shorter survival time and lower OS than low risk group (Figure S1B,S1C). The AUCs were 0.734, 0.723, and 0.773 at 1-, 2-, and 3-year respectively (Figure S1D). The squamous cell carcinoma patients also were divided into low- and high-risk groups (Figure S2A) and the same analysis were also performed. However, there was no significant difference in OS between the high- and low-risk groups of patients with squamous cell carcinoma (Figure S2B,S2C). The AUCs at 1-, 2-, 3-year were only 0.567, 0.646, and 0.524 respectively (Figure S2D). It turned out that the risk model performed better in adenocarcinoma rather than squamous cell carcinoma.

Independent prognostic value of the miRNA signature model

Subsequently, univariate and multivariate Cox regression analyses were carried out to test the role of our risk score in predicting the OS of EC patients. It was proven that the risk score was an independent prognostic indicator for the OS of EC patients in both the training cohort [P=0.02, HR =1.642, 95% confidence interval (CI): 1.082–2.492] and validation cohort (P<0.001, HR =1.652, 95% CI: 1.308–2.086) with univariate Cox regression analyses (*Figure 5A,5B*). The risk score was still an independent prognostic factor in both cohorts (training cohort: P=0.048, HR =1.483, 95% CI: 0.826–2.665; validation cohort: P<0.001, HR =1.884, 95% CI: 1.352–2.627), as confirmed by multivariate Cox regression analyses (*Figure 5C,5D*). In addition, the clinical characteristics and the expression

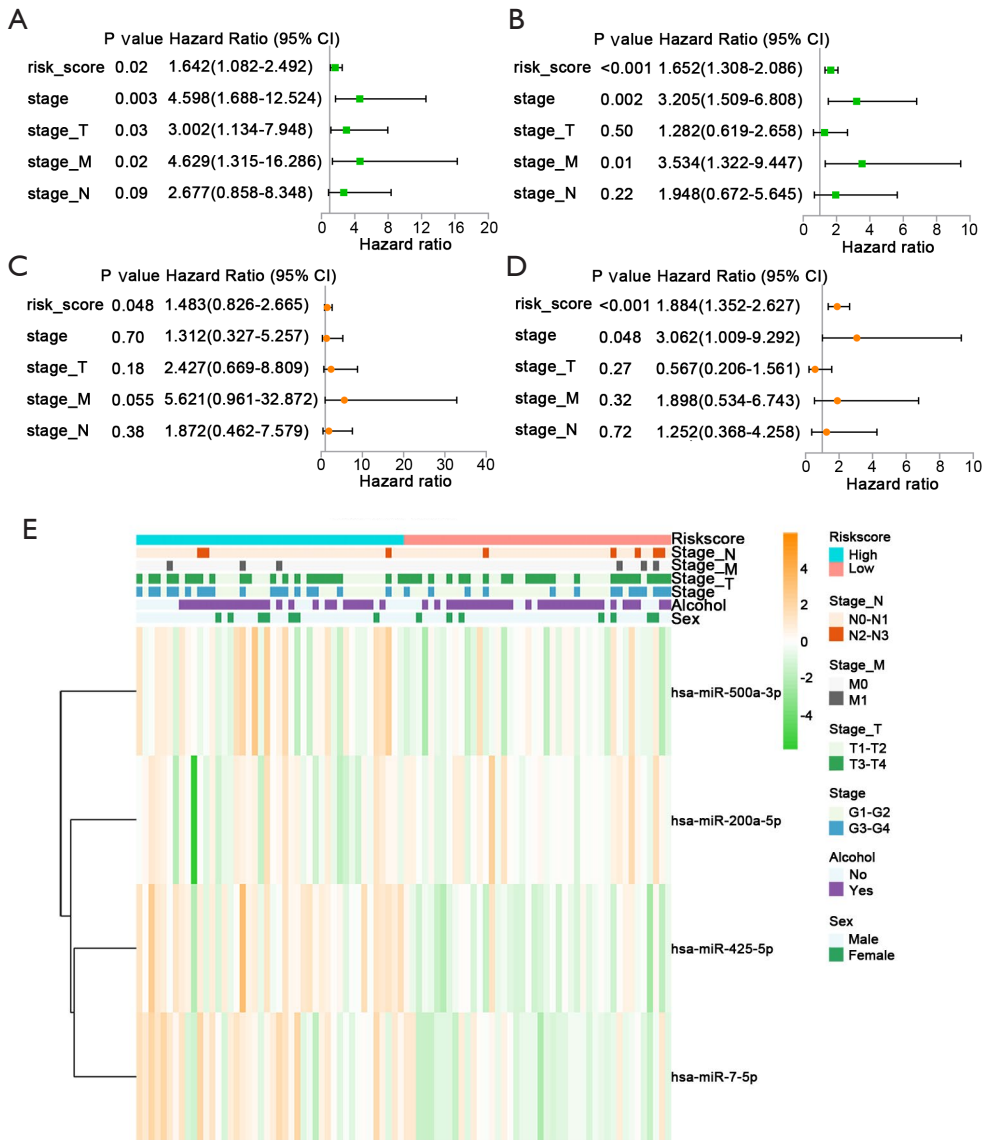

Figure 5 Independent prognostic value of the risk model. (A,C) Univariate (A) and multivariate (C) Cox analyses in the training cohort. (B,D) Univariate (B) and multivariate (D) Cox analyses in the validation cohort. (E) Heatmap of the four necroptosis-related miRNAs and clinical features in the high- and low-risk groups. CI, confidence interval; miRNAs, microRNAs.

of the four necroptosis-related miRNAs in the high- and low-risk groups of the training and validation cohorts were analysed in the heatmap, which revealed that there was no large difference in the clinical features between the high- and low-risk groups, but the expression of hsa-miR-500a-3p, hsa-miR-425-5p, and hsa-miR-7-5p was higher in the patients with high risk (*Figure 5E*).

Analysis of miRNA-target genes

From three databases (miRDB, miRTarBase and TargetScan), we collected data on the target genes of the four necroptosis-related miRNAs. After that, 165 target genes of the four necroptosis-related miRNAs were identified, as shown in the Venn diagram (*Figure 6A*). The association between miRNAs and target genes was

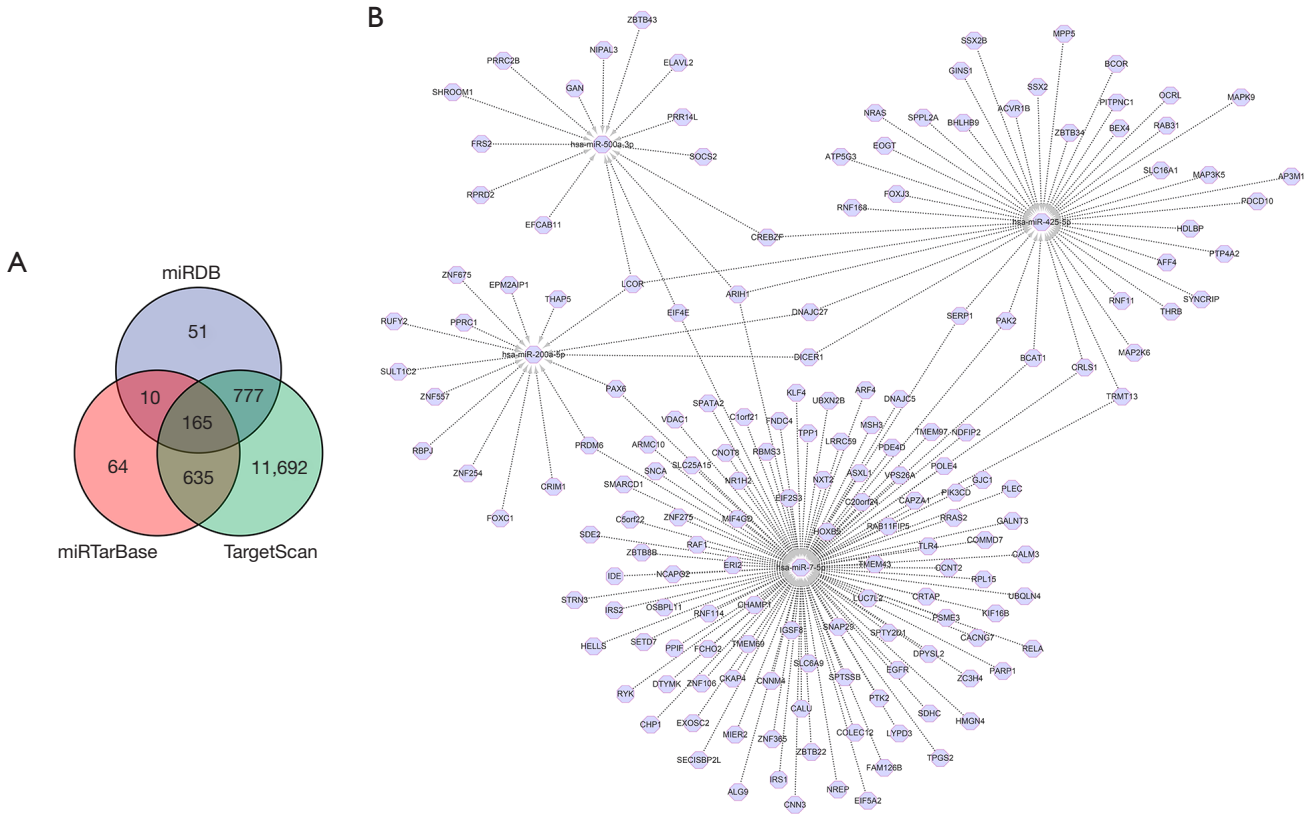

Figure 6 The target genes of the four necroptosis-related miRNAs. (A) Venn diagram of the miRNA targets predicted by miRDB, miRTarBase and TargetScan. (B) Network of four miRNAs and their target genes. miRNAs, microRNAs.

further explored with Cytoscape 3.9.1. The network of four necroptosis-related miRNA-target gene interactions was shown in *Figure 6B*.

Next, we performed underlying biological function and pathway analyses of these target genes on the basis of GO enrichment and KEGG pathway analysis. The results in the bar plot (*Figure 7A*) displayed the biological process (BP), cellular component (CC), and molecular function (MF) terms of the target genes. It was demonstrated that the target genes were significantly enriched in BP related to cellular response and metabolic process; they were mainly enriched in intracellular organelle, nucleus and cytoplasmic part for CC item, while protein binding, organic cyclic compound binding and heterocyclic compound binding for MF item. The dot plot of *Figure 7B* with KEGG analysis indicated that the associated pathways were the mitogen-activated protein kinase (MAPK) signaling pathway, the Ras signaling pathway, apoptosis, cellular senescence, PD-L1 expression and programmed cell death protein 1 (PD-1) checkpoint pathway in cancer, etc.

Effects of miR-425-5p on necroptosis and target genes in EC cell lines in vitro

The results shown above indicated that the four necroptosis-related miRNA model was fairly robust, in which the correlation of miR-425-5p with survival of EC patients was the most striking (P=0.01). The EC cell lines EC109 and EC9706 were then treated with NC inhibitor or miR-425-5p inhibitor to explore the effects of miR-425-5p on necroptosis. Flow cytometry identified that the ratio of necroptosis in the miR-425-5p inhibitor group was significantly higher than that in the control group in both two EC cell lines (necroptosis: left upper) (*Figure 8A*). The mRNA expression levels of four necroptotic markers, including *FADD* (fas-associated via death domain), *RIPK1* (receptor interacting serine/threonine-protein kinase 1), *RIPK3* (receptor interacting serine/threonine-protein kinase 3), and *MLKL* (mixed lineage kinase domain-like protein), were elevated similarly when the expression of miR-425-5p was inhibited (*Figure 8B*). There were ten target genes

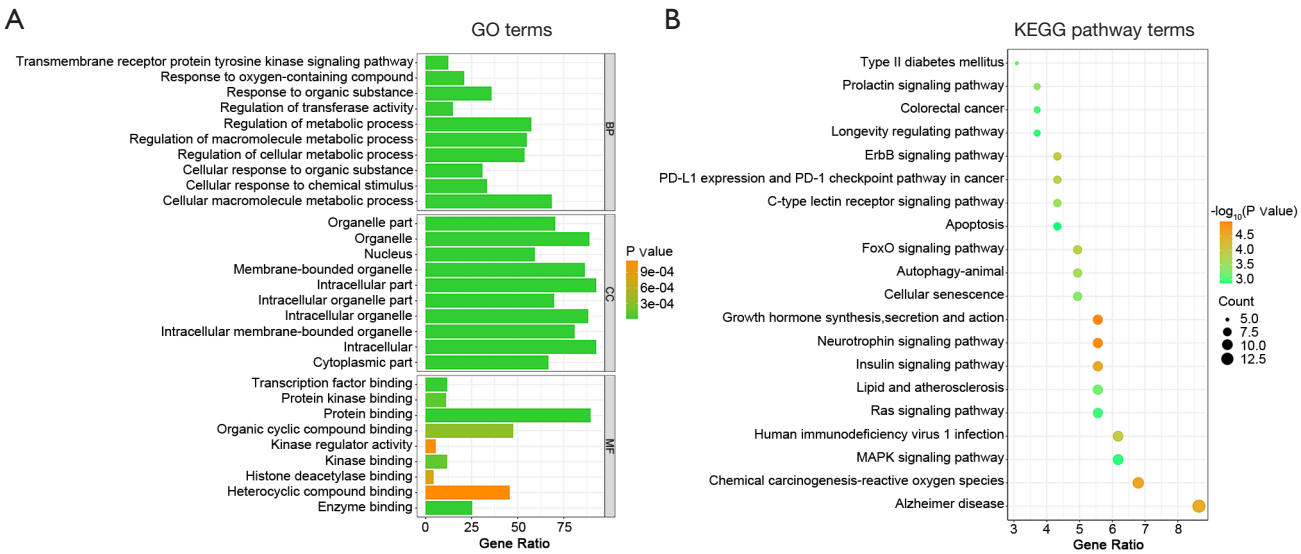

Figure 7 Functional enrichment analysis of the target genes in the TCGA cohort. (A) GO analysis of the miRNA-target genes into three functional groups, including BP, CC and MF. (B) The enriched items of the miRNA-target genes identified via KEGG analysis. GO, Gene Ontology; BP, biological process; CC, cellular component; MF, molecular function; KEGG, Kyoto Encyclopedia of Genes and Genomes; TCGA, The Cancer Genome Atlas; miRNA, microRNA.

for which miR-425-5p was in common with the other three miRNAs. The box plots showed their expression levels in tumor and normal tissue in gene expression profiling interactive analysis (GEPIA) database, in which the expression levels of *BCAT1*, *CRLS1* (cardiolipin synthase 1), *LCOR* (ligand dependent nuclear receptor corepressor), *PAK2* [P21 (RAC1) activated kinase 2] were significantly different between the tumor and normal groups (Figure S3). Then the mRNA expression levels of the target genes *PAK2*, *LCOR*, *CRLS1*, and *BCAT1* of miR-425-5p were detected to further determine the effector of miR-425-5p. The results of real-time PCR revealed that the inhibition of miR-425-5p significantly decreased the expression of *BCAT1* in both EC109 and EC9706 cells (*Figure 8C*). Taken together, these findings indicated that the inhibition of miR-425-5p promoted necroptosis in EC cells by targeting *BCAT1*.

BCAT1 was correlated with immune infiltration

Considering that PD-L1 expression and PD-1 checkpoint pathway in cancer were associated with target genes, we explored the correlation between immune infiltration and *BCAT1* expression in EC. The GSVA enrichment analysis displayed that melanogenesis, hedgehog signaling pathway, basal cell carcinoma, glycosaminoglycan biosynthesis chondroitin sulfate, glycosaminoglycan biosynthesis heparan sulfate, extracellular matrix (ECM) receptor interaction, focal adhesion, transforming growth factor-β (TGF-β) signaling pathway, melanoma, pathways in cancer, and regulation of actin cytoskeleton were significantly enriched in *BCAT1* high-expression group (*Figure 9A*). Moreover, we found that the enrichment scores of natural killer (NK) $CD56^{dim}$ cells, monocyte cells, neutrophil cells, and Th17 cells were lower in *BCAT1* high-expression group by performing ssGSEA algorithm (*Figure 9B*). As shown in *Figure 9C*, the immune checkpoints *CD276*, *TNFRSF18*, *CD274*, *CD44*, and *CD40* were more highly expressed in *BCAT1* high-expression group. Subsequently, we validated the immune infiltration results through experiments. Immunohistochemistry displayed that Ly6G+ cells (monocyte cells and neutrophil cells) were almost undetectable when BCAT1 expression was high in EC tissues (*Figure 9D*). *BCAT1* expression was reduced by the *BCAT1* inhibitor EGR240 in EC9706 cells. The results of real-time PCR and western blotting revealed that *CD274* expression was significantly decreased when the expression of *BCAT1* was inhibited (*Figure 9E,9F*).

Discussion

A few studies on necroptosis in EC have been reported. The necrosome complex *RIPK1* and *RIPK3* induce the

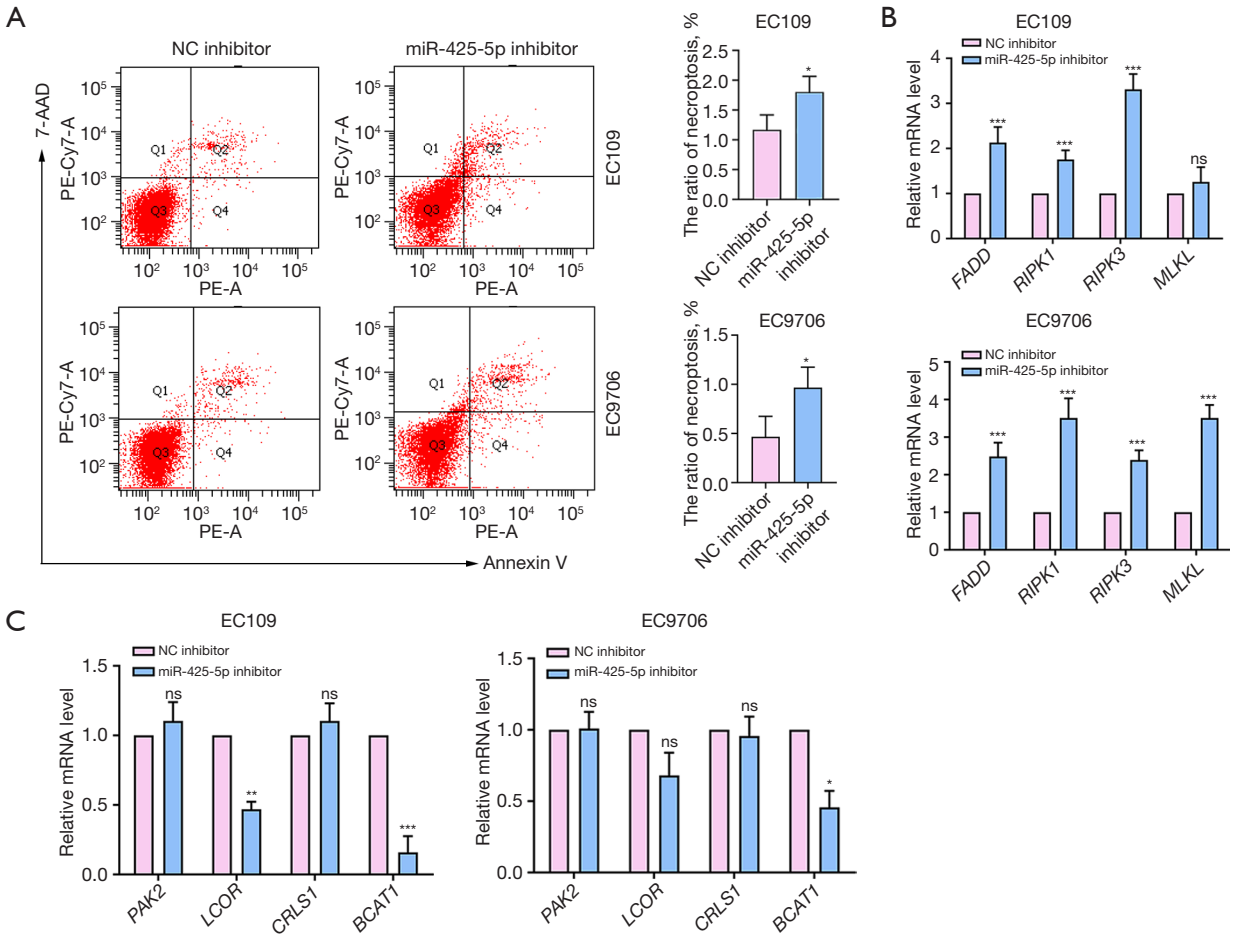

Figure 8 Effects of miR-425-5p on necroptosis and downstream target genes in EC cell lines *in vitro*. (A) Flow cytometry of EC109 and EC9706 cell lines treated with NC inhibitor or miR-425-5p inhibitor (necroptosis: left upper). (B) The expression levels of four necroptotic markers were detected by real-time PCR. (C) The expression levels of four target genes of miR-425-5p were assessed by real-time PCR. *, P<0.05; **, P<0.01; ***, P<0.001; ns, not significant. NC, negative control; *FADD*, fas associated via death domain; *RIPK1*, receptor interacting serine/threonine-protein kinase 1; *RIPK3*, receptor interacting serine/threonine-protein kinase 3; *MLKL*, mixed lineage kinase domain-like protein; *PAK2*, P21 (RAC1) activated kinase 2; *LCOR*, ligand dependent nuclear receptor corepressor; *CRLS1*, cardiolipin synthase 1; *BCAT1*, branched chain amino acid transaminase 1; EC, esophageal cancer; PCR, polymerase chain reaction.

phosphorylation of MLKL to promote necroptosis (22). *RIPK3*, the key regulator of necroptotic cell death, is significantly downregulated in EC (23). *RIPK1* facilitates ESCC cell apoptosis via activation of the c-Jun NH2-terminal kinase (JNK) pathway (24). A high status of pMLKL in ESCC patients is significantly associated with a worse prognosis and a lower therapeutic efficacy in post-neoadjuvant chemotherapy (NAC) resected specimens and pre-NAC biopsy specimens (13). However, the potential value of necroptosis-related miRNAs in the prognosis of EC still needs to be elucidated.

In our study, 13 necroptosis-related miRNAs were obtained from a previous report (21), nine of which were screened for further analysis with the corresponding miRNA expression profiles. Four necroptosis-related miRNAs (miR-425-5p, miR-500a-3p, miR-7-5p and miR-200a-5p) were subsequently used to construct an independent prognostic model in EC. Our model was proven to have great predictive performance by Kaplan-Meier survival, AUC, univariate Cox regression and multivariate Cox regression analyses. On the basis of our results, miR-425-5p, miR-500a-3p and miR-7-5p were highly expressed in

the high-risk group of EC patients, while the expression of miR-200a-5p was higher in the low-risk group with better patient survival. MiR-500a-3p suppressed the membrane translocation and phosphorylation of MLKL by binding to the 3'UTR of *MLKL* (25). MiR-7-5p (miR-7) has been reported to induce necroptosis in rhabdomyosarcoma (26). MiR-200a-5p can regulate RIP3-dependent necroptosis by targeting ring finger protein 11 (*RNF11*) (27). A study reported that miR-425-5p can inhibit the expression of *RIPK1* by targeting the 3′UTR of *RIPK1* mRNA, which results in the suppression of necroptosis (28). There is little research on these four miRNAs in EC. It was reported that the downregulation of miR-7-5p notably suppressed the progression of EC (29). MiR-425-5p has a dual role in EC. Zhidan *et al.* showed that the decreased expression of miR-425-5p inhibited the progression of EC (30), whereas Li *et al.* pointed out that miR-425-5p inhibition accelerated the progression of EC (31). However, there are no relevant reports on the role of miR-500a-3p and miR-200a-5p in EC.

We also evaluated the performance of the model in stratified groups considering that EC is a diverse entity. It turned out that the risk model performed better in adenocarcinoma than in squamous cell carcinoma. In addition, we analyzed whether stage, stage_N, stage_M, or stage_T could be independent prognostic indicators for the OS of EC patients in both the training cohort and validation cohort by univariate and multivariate Cox regression analyses. The results displayed that the stage (stage_M) was an independent prognostic factor in univariate Cox regression analyses, but not in multivariate Cox regression analyses. Our miRNA signature may be especially predictive for the adenocarcinoma patients in stage_M, which still needs to expand the sample size for further exploration. This will help our prognostic model provide more accurate services for different patient subgroups.

To further explore the molecular functions, we investigated the target genes of these necroptosis-related miRNAs. GO enrichment and KEGG analysis showed that the functions of target genes are focused on the MAPK signaling pathway, apoptosis and cellular senescence. The MAPK pathway is closely related to cell death (32). The activation of the MAPK signaling pathway has been reported to induce necroptosis (33). *RIPK1*, the key effector in necroptosis, promotes apoptosis in a time-delayed manner (34). The expression of *p16*, *p21*, and *p53*, which are markers of cellular senescence, decreases when necroptosis is inhibited (35). These evidences provide a direction for exploring the molecular mechanisms of necroptosis-related miRNAs in EC. MiR-425-5p was the most significantly correlated miRNA with survival of EC patients in our necroptosis-associated miRNA model; thus, we further detected the effect of miR-425-5p on necroptosis. Our results showed that the ratio of necroptosis in the miR-425-5p inhibitor group was significantly higher than that in the negative control group, which was also proven by Zhidan *et al.* (30). However, compared with them, our risk model has a more complete testing and validation process and contains three other miRNAs in addition to miR-425-5p, which provides a solid and stable prognostic prediction for EC patients. Furthermore, we found that the mRNA expression levels of four necroptotic markers (*FADD*, *RIPK1*, *RIPK3* and *MLKL*) were elevated in the miR-425-5p inhibitor group compared with those in the control group. A previous study has reported that tumor necroptosis is extremely important for enhancing immunogenicity and vaccine efficacy, which may become a new method for developing cancer vaccines (36). In an experimental mouse model, antitumor immunity was induced through vaccinating necroptotic cancer cells (37). MiRNAs have been reported as biomarkers of cancer diagnosis and can be used to predict drug efficacy and patient prognosis in various cancer types (38). Lin *et al.* reported that miR-23a inhibition effectively augments the antitumor function and cytotoxic potency of $CD8^+$ cytotoxic T lymphocytes (CTLs) (39). In addition, our results revealed that the target gene *BCAT1* of miR-425-5p was significantly correlated with immune infiltration. The inhibition of *BCAT1* significantly reduced *CD274* expression. MiR-425-5p inhibition may also play a role in antitumor immunity by inducing necroptosis, which might be used to treat EC in the future.

The expression levels of ten miR-425-5p target genes were subsequently analyzed in the GEPIA database, from which we filtered *BCAT1*, *CRLS1*, *LCOR* and *PAK2* with remarkably higher expression in esophageal carcinoma tissues than in normal tissues. It can be speculated that miR-425-5p may regulate the necroptosis of EC cells by targeting *BCAT1* in view of our results. Branched chain amino transaminase 1 (*BCAT1*), a key enzyme that catalyzes the metabolism of branched chain amino acid, is highly expressed in a wide variety of tumors. *BCAT1* promotes cell proliferation in melanoma (40) and hepatocellular carcinoma and can be a prognostic predictor due to its significant correlation with prognosis (41). The role of *BCAT1* in driving cell proliferation depends on its redox

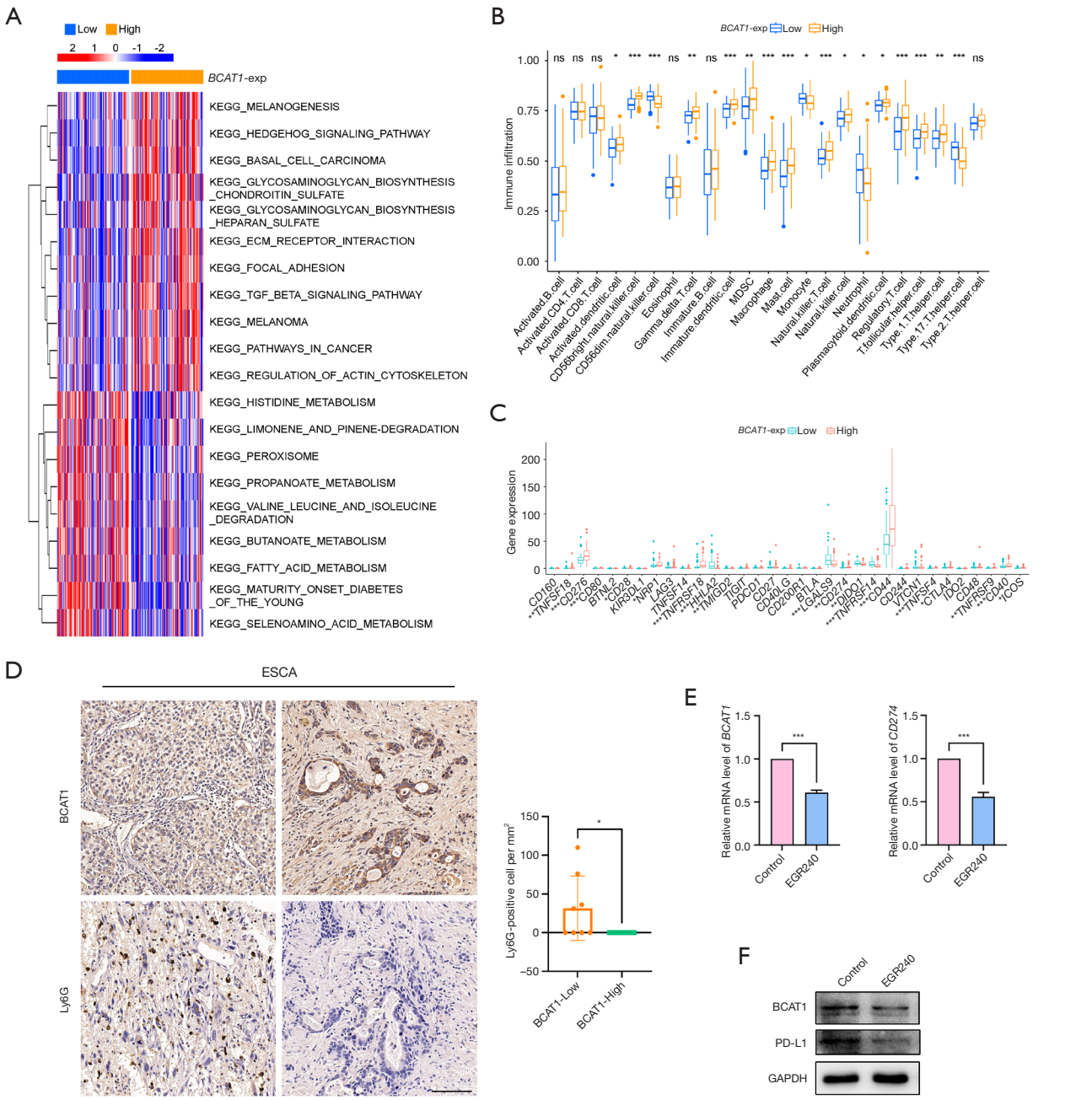

Figure 9 *BCAT1* expression and immune infiltration analysis in EC. (A) The biological pathway between the low- and high-*BCAT1* expression group by GSVA (red: activated pathways; blue: inhibited pathways). (B) Relationship between *BCAT1* expression and immune cell infiltration. (C) Analysis of immune checkpoint expression in *BCAT1* low- and high-expression group. (D) Representative images and quantification of immunohistochemistry staining of BCAT1 and Ly6G in esophageal cancer tissue microarray (scale bar: 100 μm). (E,F) The expression levels of *BCAT1* and *CD274* in EC9706 cells after EGR240 treatment were assayed by real-time PCR (E) and Western blotting (F). *, P<0.05; **, P<0.01; ***, P<0.001; ns, not significant. *BCAT1*, branched-chain amino acid transaminase 1; EC, esophageal cancer; PCR, polymerase chain reaction; GSVA, gene set variation analysis; *BCAT1*_exp, *BCAT1* expression; KEGG, Kyoto Encyclopedia of Genes and Genomes; ESCA, esophageal cancer; Ly6G, lymphocyte antigen 6G; PD-L1 (*CD274*), programmed cell death 1 ligand 1; GAPDH, glyceraldehyde-3-phosphate dehydrogenase.

function in maintaining mitotic fidelity (42). *BCAT1* overexpression promotes cell proliferation and induces c-Myc through the Wnt/β-catenin signaling pathway in lung cancer cells (43). *BCAT1* increases endometrial cancer cell proliferation through activating the expression of pS6K, a downstream target kinase of mTORC1 (44). Interestingly, in our study, we found that *BCAT1* is a target gene of necroptosis-related miR-425-5p. The inhibition of miR-425-5p decreased the expression of *BCAT1* and promoted necroptosis in EC cells. Although other mechanisms cannot be excluded, we propose that miR-425-5p may activate the Wnt/β-catenin and mTORC1 pathways by increasing *BCAT1* expression, ultimately promoting cell proliferation and decreasing necroptosis of EC cells.

In our work, we performed data analysis only in the TCGA datasets because of the lack of miRNA expression data with the corresponding clinical information in the other datasets, which is a limitation of our study. Due to the low frequency of TCGA dataset updates, there may be potential biases in this study. Despite we have utilized advanced analysis methods for machine deep learning to improve the accuracy and reliability of data analysis, we still need to continuously monitor data updates in the TCGA and collect more new EC samples for further validation of the risk model to eliminate potential biases. Furthermore, our findings rely mainly on bioinformatics analysis and still face the challenge of clinical translation. There are significant individual differences among clinical patients, which were influenced by a variety of factors, for instance, patient age, underlying diseases, lifestyle, environmental conditions and others. This makes it is extremely difficult and complex to valid the risk model in real clinical scenarios. In addition, we cannot have a definite estimate of the application effect of the model, which still needs to be confirmed by further large-scale and prospective clinical trials.

Conclusions

In conclusion, we successfully constructed a novel necroptosis-related miRNA signature to effectively predict the prognosis of EC patients, which can provide therapeutic targets for EC in the future.

Acknowledgments

We thank TCGA for their data support.

Footnote

Reporting Checklist: The authors have completed the TRIPOD reporting checklist. Available at https://tcr.amegroups.com/article/view/10.21037/tcr-24-1532/rc

Data Sharing Statement: Available at https://tcr.amegroups.com/article/view/10.21037/tcr-24-1532/dss

Peer Review File: Available at https://tcr.amegroups.com/article/view/10.21037/tcr-24-1532/prf

Funding: This study was supported by the Clinical Research Award of the First Affiliated Hospital of Xi'an Jiaotong University, China (No. XJTU1AF-CRF-2023-024), National Natural Science Foundation of China (Nos. 82173023, 82372931, 82373389).

Conflicts of Interest: All authors have completed the ICMJE uniform disclosure form (available at https://tcr.amegroups.com/article/view/10.21037/tcr-24-1532/coif). The authors have no conflicts of interest to declare.

Ethical Statement: The authors are accountable for all aspects of the work in ensuring that questions related to the accuracy or integrity of any part of the work are appropriately investigated and resolved. The study was conducted in accordance with the Declaration of Helsinki (as revised in 2013).

References

1. Bray F, Laversanne M, Sung H, et al. Global cancer statistics 2022: GLOBOCAN estimates of incidence and mortality worldwide for 36 cancers in 185 countries. CA Cancer J Clin 2024;74:229-63.
2. Harada K, Yamamoto S, Kato K. Pembrolizumab for the

treatment of advanced esophageal cancer. Future Oncol 2022;18:2311-9.
3. Huang FL, Yu SJ. Esophageal cancer: Risk factors, genetic association, and treatment. Asian J Surg 2018;41:210-5.
4. Uhlenhopp DJ, Then EO, Sunkara T, et al. Epidemiology of esophageal cancer: update in global trends, etiology and risk factors. Clin J Gastroenterol 2020;13:1010-21.
5. Degterev A, Huang Z, Boyce M, et al. Chemical inhibitor of nonapoptotic cell death with therapeutic potential for ischemic brain injury. Nat Chem Biol 2005;1:112-9.
6. Yan J, Wan P, Choksi S, et al. Necroptosis and tumor progression. Trends Cancer 2022;8:21-7.
7. Yin J, Yu Y, Huang X, et al. Necroptosis in immunity, tissue homeostasis, and cancer. Curr Opin Immunol 2024;89:102455.
8. Koo GB, Morgan MJ, Lee DG, et al. Methylation-dependent loss of RIP3 expression in cancer represses programmed necrosis in response to chemotherapeutics. Cell Res 2015;25:707-25.
9. Seifert L, Werba G, Tiwari S, et al. The necrosome promotes pancreatic oncogenesis via CXCL1 and Mincle-induced immune suppression. Nature 2016;532:245-9.
10. Jiao D, Cai Z, Choksi S, et al. Necroptosis of tumor cells leads to tumor necrosis and promotes tumor metastasis. Cell Res 2018;28:868-70.
11. Feng X, Song Q, Yu A, et al. Receptor-interacting protein kinase 3 is a predictor of survival and plays a tumor suppressive role in colorectal cancer. Neoplasma 2015;62:592-601.
12. Dong Y, Sun Y, Huang Y, et al. Upregulated necroptosis-pathway-associated genes are unfavorable prognostic markers in low-grade glioma and glioblastoma multiforme. Transl Cancer Res 2019;8:821-7.
13. Yamauchi T, Fujishima F, Hashimoto M, et al. Necroptosis in Esophageal Squamous Cell Carcinoma: An Independent Prognostic Factor and Its Correlation with Tumor-Infiltrating Lymphocytes. Cancers (Basel) 2021;13:4473.
14. Chipman LB, Pasquinelli AE. miRNA Targeting: Growing beyond the Seed. Trends Genet 2019;35:215-22.
15. Yin Z, Wang W, Qu G, et al. MiRNA-96-5p impacts the progression of breast cancer through targeting FOXO3. Thorac Cancer 2020;11:956-63.
16. Sur S, Steele R, Shi X, et al. miRNA-29b Inhibits Prostate Tumor Growth and Induces Apoptosis by Increasing Bim Expression. Cells 2019;8:1455.
17. Han DL, Wang LL, Zhang GF, et al. MiRNA-485-5p, inhibits esophageal cancer cells proliferation and invasion by down-regulating O-linked N-acetylglucosamine transferase. Eur Rev Med Pharmacol Sci 2019;23:2809-16.
18. Song J, Zhang P, Liu M, et al. Novel-miR-4885 Promotes Migration and Invasion of Esophageal Cancer Cells Through Targeting CTNNA2. DNA Cell Biol 2019;38:151-61.
19. Cai Y, Xia L, Zhu H, et al. MiR-3682-3p promotes esophageal cancer progression by targeting FHL1 and activating the Wnt/β-catenin signaling pathway. Cell Signal 2024;119:111155.
20. Li K, Lin Y, Zhou Y, et al. Salivary Extracellular MicroRNAs for Early Detection and Prognostication of Esophageal Cancer: A Clinical Study. Gastroenterology 2023;165:932-945.e9.
21. Liu Y, Chen Q, Zhu Y, et al. Non-coding RNAs in necroptosis, pyroptosis and ferroptosis in cancer metastasis. Cell Death Discov 2021;7:210.
22. Shimizu K, Inuzuka H, Tokunaga F. The interplay between cell death and senescence in cancer. Semin Cancer Biol 2025;108:1-16.
23. Sun Y, Zhai L, Ma S, et al. Down-regulation of RIP3 potentiates cisplatin chemoresistance by triggering HSP90-ERK pathway mediated DNA repair in esophageal squamous cell carcinoma. Cancer Lett 2018;418:97-108.
24. Zhang Y, Du J, Duan X, et al. RIPK1 contributes to cisplatin-induced apoptosis of esophageal squamous cell carcinoma cells via activation of JNK pathway. Life Sci 2021;269:119064.
25. Jiang L, Liu XQ, Ma Q, et al. hsa-miR-500a-3P alleviates kidney injury by targeting MLKL-mediated necroptosis in renal epithelial cells. FASEB J 2019;33:3523-35.
26. Yang L, Kong D, He M, et al. MiR-7 mediates mitochondrial impairment to trigger apoptosis and necroptosis in Rhabdomyosarcoma. Biochim Biophys Acta Mol Cell Res 2020;1867:118826.
27. Yang T, Cao C, Yang J, et al. miR-200a-5p regulates myocardial necroptosis induced by Se deficiency via targeting RNF11. Redox Biol 2018;15:159-69.
28. Gu C, Hou C, Zhang S. miR-425-5p improves inflammation and septic liver damage through negatively regulating the RIP1-mediated necroptosis. Inflamm Res 2020;69:299-308.
29. Shi W, Song J, Gao Z, et al. Downregulation of miR-7-5p Inhibits the Tumorigenesis of Esophagus Cancer via Targeting KLF4. Onco Targets Ther 2020;13:9443-53.
30. Zhidan X, Kedi X, Dan X, et al. Predictive and Carcinogenic Roles of Necroptosis-Related miR-425-5p and miR-16-5p in Esophageal Squamous Cell Carcinoma.

Ann Clin Lab Sci 2024;54:76-85.
31. Li P, Ding H, Han S, et al. Long noncoding RNA LINC00858 aggravates the progression of esophageal squamous cell carcinoma via regulating the miR-425-5p/ABL2 axis. Heliyon 2024;10:e27337.
32. Villa E, Paul R, Meynet O, et al. The E3 ligase UBR2 regulates cell death under caspase deficiency via Erk/MAPK pathway. Cell Death Dis 2020;11:1041.
33. Tang X, Fan X, Xu T, et al. Polystyrene nanoplastics exacerbated lipopolysaccharide-induced necroptosis and inflammation via the ROS/MAPK pathway in mice spleen. Environ Toxicol 2022;37:2552-65.
34. Naito MG, Xu D, Amin P, et al. Sequential activation of necroptosis and apoptosis cooperates to mediate vascular and neural pathology in stroke. Proc Natl Acad Sci U S A 2020;117:4959-70.
35. Thadathil N, Selvarani R, Mohammed S, et al. Senolytic treatment reduces cell senescence and necroptosis in Sod1 knockout mice that is associated with reduced inflammation and hepatocellular carcinoma. Aging Cell 2022;21:e13676.
36. Tong X, Tang R, Xiao M, et al. Targeting cell death pathways for cancer therapy: recent developments in necroptosis, pyroptosis, ferroptosis, and cuproptosis research. J Hematol Oncol 2022;15:174.
37. Aaes TL, Kaczmarek A, Delvaeye T, et al. Vaccination with Necroptotic Cancer Cells Induces Efficient Anti-tumor Immunity. Cell Rep 2016;15:274-87.
38. Kim T, Croce CM. MicroRNA: trends in clinical trials of cancer diagnosis and therapy strategies. Exp Mol Med 2023;55:1314-21.
39. Lin R, Chen L, Chen G, et al. Targeting miR-23a in CD8+ cytotoxic T lymphocytes prevents tumor-dependent immunosuppression. J Clin Invest 2014;124:5352-67.
40. Zhang B, Xu F, Wang K, et al. BCAT1 knockdown-mediated suppression of melanoma cell proliferation and migration is associated with reduced oxidative phosphorylation. Am J Cancer Res 2021;11:2670-83.
41. Zheng YH, Hu WJ, Chen BC, et al. BCAT1, a key prognostic predictor of hepatocellular carcinoma, promotes cell proliferation and induces chemoresistance to cisplatin. Liver Int 2016;36:1836-47.
42. Francois L, Boskovic P, Knerr J, et al. BCAT1 redox function maintains mitotic fidelity. Cell Rep 2022;41:111524.
43. Lin X, Tan S, Fu L, et al. BCAT1 Overexpression Promotes Proliferation, Invasion, and Wnt Signaling in Non-Small Cell Lung Cancers. Onco Targets Ther 2020;13:3583-94.
44. Wang P, Wu S, Zeng X, et al. BCAT1 promotes proliferation of endometrial cancer cells through reprogrammed BCAA metabolism. Int J Clin Exp Pathol 2018;11:5536-46.

Cite this article as: Zhang M, Song S, Wang B, Shang Y, Liu P, Li J. A novel necroptosis-related miRNA signature for predicting the prognosis of esophageal cancer and immune infiltration analysis. Transl Cancer Res 2025;14(2):949-965. doi: 10.21037/tcr-24-1532